J Biomol NMR (2007) 38:315–324
DOI 10.1007/s10858-007-9171-9

ARTICLE

Model-free analysis for large proteins at high magnetic field strengths

Shou-Lin Chang · Andrew P. Hinck · Rieko Ishima

Received: 30 March 2007 / Accepted: 21 May 2007 / Published online: 26 June 2007

Abstract Protein backbone dynamics is often characterized using model-free analysis of three sets of ^{15}N relaxation data: longitudinal relaxation rate (R_1), transverse relaxation rate (R_2), and ^{15}N–{H} NOE values. Since the experimental data is limited, a simplified model-free spectral density function is often used that contains one Lorentzian describing overall rotational correlation but not one describing internal motion. The simplified spectral density function may be also used in estimating the overall rotational correlation time, by making the R_2/R_1 largely insensitive to internal motions, as well as used as one of the choices in the model selection protocol. However, such approximation may not be valid for analysis of relaxation data of large proteins recorded at high magnetic field strengths since the contribution to longitudinal relaxation from the Lorentzian describing the overall rotational diffusion of the molecule is comparably small relative to that describing internal motion. Here, we quantitatively estimate the errors introduced by the use of the simplified spectral density in model-free analysis for large proteins at high magnetic field strength.

S.-L. Chang
Institute of Bioinformatics and Structural Biology, Department of Life Science, National Tsing Hua University, HsinChu 30055, Taiwan

A. P. Hinck
Department of Biochemistry, MC 7760, University of Texas Health Science Center at San Antonio, San Antonio, TX 78229-3900, USA

R. Ishima (✉)
Department of Structural Biology, School of Medicine, University of Pittsburgh, Rm 1037, Biomedical Science Tower 3, 3501 Fifth Avenue, Pittsburgh, PA 15260, USA
e-mail: ishima@pitt.edu

Keywords NMR · Relaxation · Rotational correlation time · Protein · Dynamics

Introduction

NMR relaxation is often applied to characterize protein internal motion (Bruschweiler 2003; Dayie et al. 1996; Fushman and Cowburn 2001; Igumenova et al. 2006; Ishima and Torchia 2000; Jarymowycz and Stone 2006; Kay 2005; Palmer 2001; Redfield 2004). To evaluate internal motion on the sub-nanosecond time scale, model-free analysis is one of the most frequently used approaches (Lipari and Szabo 1982). Particularly in the characterization of backbone dynamics of proteins, three types of ^{15}N relaxation data, longitudinal (R_1), transverse relaxation rates (R_2), and ^{15}N–{H} NOE are typically used in the analysis to optimize the model-free parameters by χ^2 minimization of a target function (Clore et al. 1990; Kay et al. 1989; Mandel et al. 1995; Palmer et al. 1991; Schneider et al. 1992). Although inclusion of other relaxation data sets, such as cross-correlation relaxation rates, auto-relaxation rates at different static or effective magnetic field strengths, or relaxation rates for different nuclei, is useful for optimization of model-free parameters (Campbell et al. 2000; Fushman et al. 1999; Idiyatullin et al. 2003; Kroenke et al. 1998; Lee et al. 1997; Pelupessy et al. 2003; Tjandra et al. 1995), the model-free analysis that uses only ^{15}N R_1, R_2, and NOE data sets has been most accepted as a global standard for straightforward characterization of protein backbone dynamics.

There are two major steps in the model-free analysis using ^{15}N R_1, R_2, and NOE data sets: (1) determination of a rotational correlation time(s) of a molecule (τ_R) and (2) optimization of model-free parameters at individual amide

sites. In the first step, τ_R value is often optimized by directly calculating it from the average, or trimmed R_2/R_1 ratio since the R_2/R_1 ratio is free from the effects of internal motion for sites that have short correlation time for internal motion (Fushman et al. 1994; Kay et al. 1989; Palmer et al. 1991). Alternatively, τ_R value can be optimized by fitting with a model-free spectral density function for sites that exhibit average R_2/R_1 ratios (Clore et al. 1990; Schneider et al. 1992). In the second step, typically four parameters are optimized for each site: a generalized order parameter (S^2), a correlation time for internal motion (τ_i), a chemical exchange term (R_{ex}) and a generalized order parameter for internal motion much faster than τ_i (S_f^2). This however cannot be done simultaneously with a limited number of experimental data sets. Instead, a model selection protocol is used to select one out of the five models that contain one to three of the four model-free parameters. Although there are several different protocols for model selection, the basic principle of the model-free analysis is similar in all cases (Andrec et al. 1999; Clore et al. 1990; Farrow et al. 1994; Lee and Wand 1999; Mandel et al. 1995; Spyracopoulos 2006).

The application of the model-free analysis for backbone dynamics has been mostly optimized for ^{15}N R_1, R_2, and NOE data sets acquired at the magnetic field strengths of 11.74 T (500 MHz ^{1}H) or 14.09 T (600 MHz ^{1}H). The general protocol for the model-free analysis may not necessarily be suitable for the relaxation data recorded at higher magnetic field strengths, such as 18.8 T (800 MHz ^{1}H) or higher. In addition, treatment of relaxation data from larger proteins poses an extra challenge since, except for J(0), the magnitude of the spectral density function due to molecular rotation decreases as the molecular size increases. Although many studies have been published to assess the protocols of the model-free analysis and address the accuracy of the obtained parameters (Andrec et al. 1999; Barchi et al. 1994; Chandrasekhar et al. 1992; Chen et al. 2004; d'Auvergne and Gooley 2003; Korchuganov et al. 2004; Korzhnev et al. 1997; Lee and Wand 1999; Meirovitch et al. 2003; Pawley et al. 2001; Schramm et al. 1991; Spyracopoulos 2006), none have specifically targeted the large-molecule high-field case. A previous study performed by Tjandra's group commented about errors caused by the use of R_2/R_1 ratio to estimate τ_R, but did not systematically characterize them as a function of the applied magnetic field strength (Chang and Tjandra 2005). Since, spectral density values are dependent on the static magnetic field strength and the rotational correlation time of the molecule, it is important to reexamine the assumptions used in the model-free analysis for large molecules at high magnetic field strengths.

Here, we numerically simulate relaxation rates assuming different spectral density functions, and describe the accuracy of the model-free analysis at high magnetic field strength for large proteins. We show that the use of a simplified spectral density function containing only one Lorentzian introduces potential errors in the analysis, that is, the τ_R value calculated from the average, or trimmed R_2/R_1 ratio tends to be systematically smaller than expected, which in turn results in systematic increases in the S^2 values. Similarly, the use of the one Lorentzian spectral density function will also overestimate NOE values for large proteins, which will increase the number of residues that cannot be optimized by model-free analysis. Although the discrepancies due to one Lorentzian term are negligible if τ_i values are small (< 10 ps), they become significant when the τ_i values are 20–30 ps or more due to the fact that contributions from τ_R and τ_i become comparable. These results are significant as an increasing number of proteins are being studied at high field and as τ_i values of 20–30 ps are rather commonplace even in rigid portions of proteins (Barchi et al. 1994; Chandrasekhar et al. 1992; Farrow et al. 1994; Philippopoulos et al. 1997; Sheinerman and Brooks 1997).

Methods

The relaxation rates can be expressed in terms of the spectral density function, $J(\omega)$, as described below.

$$R_1 = (d^2/10)\{3J(\omega_N) + J(\omega_H - \omega_N) + 6J(\omega_H + \omega_N)\} + c^2 J(\omega_N) \quad (1)$$

$$R_2 = (d^2/20)\{4J(0) + 3J(\omega_N) + J(\omega_H - \omega_N) + 6J(\omega_H) + 6J(\omega_H + \omega_N)\} + (c^2/3)\{4J(0) + 3J(\omega_N)\} + R_{ex} \quad (2)$$

$$\mathrm{NOE} = 1 + \{\gamma_H (d^2/10)\sigma_{cross}\}/(\gamma_N R_1) \quad (3)$$

Here, d^2 and c^2 are coefficients for dipolar and CSA interactions, and, γ_H and γ_N are gyromagnetic ratios of ^{1}H and ^{15}N, respectively, σ_{cross} is a cross relaxation term given by $(d^2/10)(6J(\omega_H + \omega_N) - J(\omega_H - \omega_N))$, and R_{ex} is the chemical exchange contribution to R_2 value (Cavanagh et al. 1996).

The typical spectral density functions applied in the model-free analysis are the simplified spectral density function, $J_{SMF}(\omega)$ (Eq. 4), the model-free spectral density function, $J_{MF}(\omega)$ (Eq. 5), and the extended spectral density function, $J_{EMF}(\omega)$ (Eq. 6).

$$J_{\mathrm{SMF}}(\omega) = S^2 \frac{\tau_{\mathrm{R}}}{(1+\omega^2\tau_{\mathrm{R}}^2)} \tag{4}$$

$$J_{\mathrm{MF}}(\omega) = S^2 \frac{\tau_{\mathrm{R}}}{(1+\omega^2\tau_{\mathrm{R}}^2)} + \left(1-S^2\right)\frac{\tau_{\mathrm{e}}}{\left(1+\omega^2\tau_{\mathrm{e}}^2\right)} \tag{5}$$

$$J_{\mathrm{EMF}}(\omega) = S_{\mathrm{f}}^2\left[S_{\mathrm{S}}^2 \frac{\tau_{\mathrm{R}}}{(1+\omega^2\tau_{\mathrm{R}}^2)} + \left(1-S_{\mathrm{S}}^2\right)\frac{\tau_{\mathrm{e}}}{\left(1+\omega^2\tau_{\mathrm{e}}^2\right)}\right] \tag{6}$$

Here, $S^2 = S_{\mathrm{f}}^2 S_{\mathrm{S}}^2$ and $\tau_{\mathrm{e}}^{-1} = \tau_{\mathrm{R}}^{-1} + \tau_{\mathrm{i}}^{-1}$. The spin coefficient, 2/5, is included in c^2 and d^2 terms for simplification. When $J_{\mathrm{SMF}}(\omega)$ and $J_{\mathrm{MF}}(\omega)$ are employed, there are options to account for chemical exchange (R_{ex}) in R_2, as described in Eq. 2. Thus, there are a total of five possible combinations of spectral densities to be selected for optimization of the model-free parameters at each amide site. The five spectral densities have the following sets of parameters: (S^2), (S^2, τ_{e}), (S^2, R_{ex}), (S^2, τ_{e}, R_{ex}), and (S^2, S_{f}^2, τ_{e}).

Approximation of $J_{\mathrm{MF}}(\omega)$ by $J_{\mathrm{SMF}}(\omega)$ is valid when the condition indicated in Eq. 7 is satisfied at all angular frequencies that contribute to relaxation, i.e., at 0, ω_{N}, and ω_{H}. Here, ω_{H} is used to approximate ($\omega_{\mathrm{H}} + \omega_{\mathrm{N}}$) and ($\omega_{\mathrm{H}} - \omega_{\mathrm{N}}$) because ω_{H} is ca. 10 times larger than ω_{N}.

$$S_{\mathrm{S}}^2 \frac{\tau_{\mathrm{R}}}{(1+\omega^2\tau_{\mathrm{R}}^2)} \gg \left(1-S_{\mathrm{S}}^2\right)\frac{\tau_{\mathrm{e}}}{\left(1+\omega^2\tau_{\mathrm{e}}^2\right)} \tag{7}$$

Under condition (7), the R_2/R_1 ratio is independent of S^2 and τ_{i} and depends solely on ω_{i} (i = H or N) and τ_{R}. Therefore, τ_{R} is directly calculated from R_2/R_1 for the sites which satisfy condition (7) (Fushman et al. 1994; Kay et al. 1989; Palmer et al. 1991). Alternatively, τ_{R} can be optimized by fitting with the model-free spectral density ($J_{\mathrm{MF}}(\omega)$) for the sites that fall around the trimmed mean R_2/R_1 ratio (Clore et al. 1990; Schneider et al. 1992).

In the case of $J(0)$ term, $J_{\mathrm{MF}}(\omega)$ is expressed according to Eq. 8.

$$J_{\mathrm{MF}}(0) = S_{\mathrm{S}}^2\tau_{\mathrm{R}} + \left(1-S_{\mathrm{S}}^2\right)\tau_{\mathrm{e}} \tag{8}$$

Therefore, condition (7) is valid simply when $\tau_{\mathrm{R}} \gg \tau_{\mathrm{e}}$. However, in the case of $J_{\mathrm{MF}}(\omega)$ at ω_{N} and ω_{H} angular frequencies, the validity of condition (7) will also depend on ω *and* τ_{R} values.

To investigate errors introduced by the use of simplified $J_{\mathrm{SMF}}(\omega)$, we first simulate $\tau/(1+\omega^2\tau^2)$ values as a function of the correlation time, τ, at individual ω_{N} and ω_{H} frequencies and at 11.74 and 18.8 T. Next, we simulate the relaxation rates expressed by Eqs. 1–3 using both $J_{\mathrm{SMF}}(\omega)$ and $J_{\mathrm{MF}}(\omega)$ spectral density functions. In the simulations of relaxation rates, we assume $S^2 = 0.85$, $\tau_{\mathrm{i}} = 10$ ps or 50 ps, and $R_{\mathrm{ex}} = 0$. According to previous studies (Barchi et al. 1994; Chandrasekhar et al. 1992; Farrow et al. 1994; Philippopoulos et al. 1997; Sheinerman and Brooks 1997), $\tau_{\mathrm{i}} = 10$ ps should be fast enough to apply $J_{\mathrm{SMF}}(\omega)$ whereas $\tau_{\mathrm{i}} = 50$ ps should fall on the border between fast and slow internal motion. NOE values in rigid regions of proteins are often larger than 0.8 when τ_{i} is 10 ps or faster (Coles et al. 1999; Ding et al. 2005; Garcia et al. 2000; Savard and Gagne 2006; Yuan et al. 1999), but in some cases lower than 0.8 when τ_{i} values are slower, i.e., $\tau_{\mathrm{i}} > 10$ ps (Abu-Abed et al. 2004; Bouamr et al. 2005; Fausti et al. 2001; Zhuravleva et al. 2004). To test the effects of static magnetic field strength, simulations were performed at 11.74 T (500 MHz ^{1}H) and 18.8 T (800 MHz ^{1}H). The simulated results are shown as a function of a rotational correlation time, τ_{R}. Simulations were performed using MATLAB (The Mathworks Inc., Natick, MA).

Results and discussion

Angular frequency dependence of the $\tau/(1+\omega^2\tau^2)$ term

The purpose of this manuscript is to determine whether the $J_{\mathrm{SMF}}(\omega)$ can be safely applied as a simplified form of $J_{\mathrm{MF}}(\omega)$ for large proteins at high magnetic field strengths. For this purpose, we do not assume molecular anisotropy, chemical exchange, or experimental noise error, but simply compare differences in relaxation values calculated using $J_{\mathrm{SMF}}(\omega)$ (Eq. 4) and $J_{\mathrm{MF}}(\omega)$ (Eq. 5). Prior to the comparison of relaxation rates, it is useful to estimate the ranges of the correlation time that satisfy the condition (7). To do so, $\tau/(1+\omega^2\tau^2)$ is plotted as a function of a general correlation time, τ, at individual ω_{N} and ω_{H} at 11.74 T and compared to $\tau/(1+\omega^2\tau^2)$ at 18.8 T (Fig. 1).

Figure 1 shows that at 10 ns overall correlation time, which corresponds roughly to a protein of 20 kDa at 25 °C (Dayie et al. 1996), the $J(\omega_{\mathrm{N}})$ at 18.8 T is only 40% of the $J(\omega_{\mathrm{N}})$ at 11.74 T. This is because the magnitude of the spectral density function is reduced when the magnetic field strength increases. On the other hand, for short correlation times, i.e., $\omega_{\mathrm{N}}\tau \ll 1$, $J(\omega_{\mathrm{N}})$ is determined by the τ term and is independent of the value of ω_{N}. Such observations indicate that once the static magnetic field increases, the magnitude of $\tau_{\mathrm{R}}/(1+\omega_{\mathrm{N}}^2\tau_{\mathrm{R}}^2)$ term (left term in condition (7)) decreases relative to $\tau_{\mathrm{e}}/(1+\omega_{\mathrm{N}}^2\tau_{\mathrm{e}}^2)$ (right term in condition (7)) in $J_{\mathrm{MF}}(\omega_{\mathrm{N}})$, suggesting that quantitative investigation of the validity of $J_{\mathrm{SMF}}(\omega)$ is required. For example, the simulation shows that when $\tau_{\mathrm{R}} = 10$ ns, $\tau_{\mathrm{i}} = 50$ ps, and $S^2 = 0.85$, the $(1-S^2)\tau_{\mathrm{e}}/(1+\omega_{\mathrm{N}}^2\tau_{\mathrm{e}}^2)$ term is only 1.1% of the $S^2\tau_{\mathrm{R}}/(1+\omega_{\mathrm{N}}^2\tau_{\mathrm{R}}^2)$ at 11.74 T, whereas it is 2.8% at 18.8 T. Similarly, when the value of τ_{R} increases,

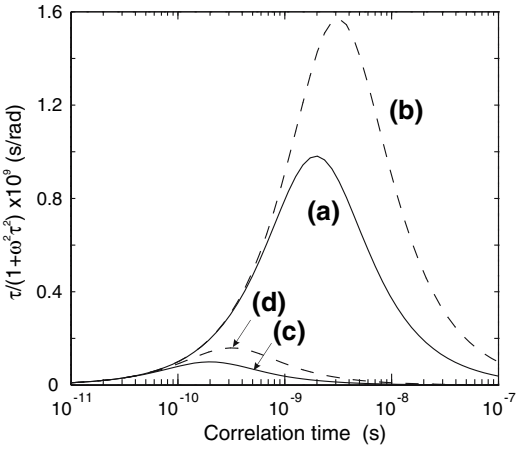

Fig. 1 Values of $\tau/(1 + \omega^2 \tau^2)$ term as a function of the correlation time, τ, (**a**) for $\omega = \omega_N$ at 18.8 T, (**b**) for $\omega = \omega_N$ at 11.74 T, (**c**) for $\omega = \omega_H$ at 18.8 T, and (**d**) for $\omega = \omega_H$ at 11.74 T

the magnitude of $\tau_R/(1 + \omega_N^2\tau_R^2)$ decreases: at τ_R = 20 ns, τ_i = 50 ps, S^2 = 0.85, the $(1 - S^2)\tau_e/(1 + \omega_N^2\tau_e^2)$ term becomes 1.8% of the $S^2\tau_R/(1 + \omega_N^2\tau_R^2)$ at 11.74 T, whereas it is 4.4% at 18.8 T.

In the case of the $J(\omega_H)$ term, condition (7) is not satisfied unless τ_i < 1 ps and τ_R < 5 ns. Nevertheless, $J_{SMF}(\omega)$ is appropriate since the overall $J(\omega_H)$ contributes little compared to $J(\omega_N)$ and $J(0)$ in R_1 and R_2 (Eqs. 1 and 2, respectively) since ω_H is ca. 10 times ω_N. However, the difference between $J_{SMF}(\omega_H)$ and $J_{MF}(\omega_H)$ is almost equivalent to that of $J_{SMF}(\omega_N)$ and $J_{MF}(\omega_N)$.

These observations suggest that there might be systematic errors caused by the optimization of model-free parameters using $J_{SMF}(\omega)$. This follows from the fact that although contributions from the $J(0)$, $J(\omega_N)$, and $J(\omega_H)$ term are different in the relaxation rates, the $S^2\tau_R/(1 + \omega_N^2\tau_R^2)$ term in the use of $J_{SMF}(\omega)$ has to compensate for the neglect of the $(1 - S^2)\tau_e/(1 + \omega_H^2\tau_e^2)$ term when condition (7) is not satisfied. Since τ_R is a global parameter, the use of $J_{SMF}(\omega)$ eventually leads to an overestimation of S^2 value when condition (7) is not satisfied.

R_1 values simulated using $J_{SMF}(\omega)$ and $J_{MF}(\omega)$

To understand how relaxation rates are dependent on the choice of the spectral density function, we simulated R_1 values (Eq. 1) using $J_{SMF}(\omega)$ and $J_{MF}(\omega)$. In this simulation, relaxation rates are shown as a function of τ_R in which τ_i and S^2 are assumed to be 50 ps and 0.85, respectively. Simulations were done at both 11.74 and 18.8 T.

Figure 2a shows that R_1 values calculated assuming $J_{SMF}(\omega)$, R_1^{SMF}, are slightly smaller than those of $J_{MF}(\omega)$, R_1^{MF}, due to the loss of $(1 - S^2)\tau_e/(1 + \omega_N^2\tau_e^2)$ term. However, the overall profile of R_1^{SMF} values as a function of τ_R is similar to that of R_1^{MF}. Relative differences in R_1^{SMF} and R_1^{MF} become larger at higher τ_R values due to the reduction of R_1 value as a function of τ_R at τ_R > 3 ns (Fig. 2a). Similar profiles are observed at both 11.74 and 18.8 T.

To evaluate the differences in R_1^{SMF} and R_1^{MF} more quantitatively, the relative difference, $(R_1^{SMF} - R_1^{MF})/R_1^{MF}$, is shown at τ_i = 10 ps and 50 ps in Fig. 3. At τ_i = 10 ps, which has been "safely" assumed to be the time constant of internal motion in the rigid regions of proteins (Fig. 3a), the $(R_1^{SMF} - R_1^{MF})/R_1^{MF}$ is ca. 1% at 11.74 T but increases to 2.5% at 18.8 T when τ_R = 20 ns. The 2.5% error is comparable to the experimental errors in R_1. Such results demonstrate that the use of $J_{SMF}(\omega)$ is valid at low magnetic field strength, but becomes marginal at the high magnetic field strength.

Although it is often assumed that fast internal motion on the time scale of τ_i < 20 ps can be neglected, (Barchi et al. 1994; Chandrasekhar et al. 1992; Mandel et al. 1995), there is experimental evidence showing internal motions on the time scale of 20–50 ps in the core regions of some proteins (Farrow et al. 1994; Sheinerman and Brooks 1997; Stone et al. 1993). Thus, it is important to account for the bias introduced into the relaxation rates when $J_{SMF}(\omega)$ is used in the analysis. As anticipated, $(R_1^{SMF}–R_1^{MF})/R_1^{MF}$ values at τ_i = 50 ps (Fig. 3b) becomes larger than those at τ_i = 10 ps (Fig. 3a). At 11.74 T, the $(R_1^{SMF} - R_1^{MF})/R_1^{MF}$ values are 2.6% and 5.0% at τ_R = 10 and 20 ns, respectively. At 18.8 T, the $(R_1^{SMF} - R_1^{MF})/R_1^{MF}$ become 5.2% and 9.6% at τ_R = 10 and 20 ns, respectively. It is noteworthy that bias introduced by $J_{SMF}(\omega)$ is significant at higher magnetic field (18.8 T) even when τ_i < 50 ps (Table 1).

NOE values simulated using $J_{SMF}(\omega)$ and $J_{MF}(\omega)$

More severe differences in the use of $J_{SMF}(\omega)$ and $J_{MF}(\omega)$ are shown for ^{15}N–{^{1}H} NOE values (Fig. 2b). The discrepancies between NOE values calculated using $J_{SMF}(\omega)$, NOE^{SMF}, and NOE values calculated using $J_{MF}(\omega)$, NOE^{MF} increase significantly as a function of τ_R (Fig. 2b). This is likely because the NOE values are largely influenced by $J(\omega_H)$ terms as shown in Eq. 3. As discussed in the previous section, the $(1–S^2)\tau_e/(1 + \omega_H^2\tau_e^2)$ term can easily become larger than $S^2\tau_R/(1 + \omega_H^2\tau_R^2)$ at τ_i larger than 1 ps when the spectral density function is evaluated at ω_H.

Differences in the NOE values, $(NOE^{SMF}–NOE^{MF})/NOE^{MF}$, shown in Fig. 4a, clearly indicate that even when τ_i = 10 ps at 11.74 T, NOE^{SMF} differs from NOE^{MF} by 3% and 5% at τ_R = 10 and 20 ns, respectively. At 18.8 T, the NOE^{SMF} differs from NOE^{MF} by 10% at τ_R = 20 ns. Furthermore, when τ_i = 50 ps (Fig. 4b), the NOE^{SMF} differs from NOE^{MF} by more than 10% and 30% at 11.74 T and 18.8 T, respectively, even at τ_R = 10 ns. Although NOE

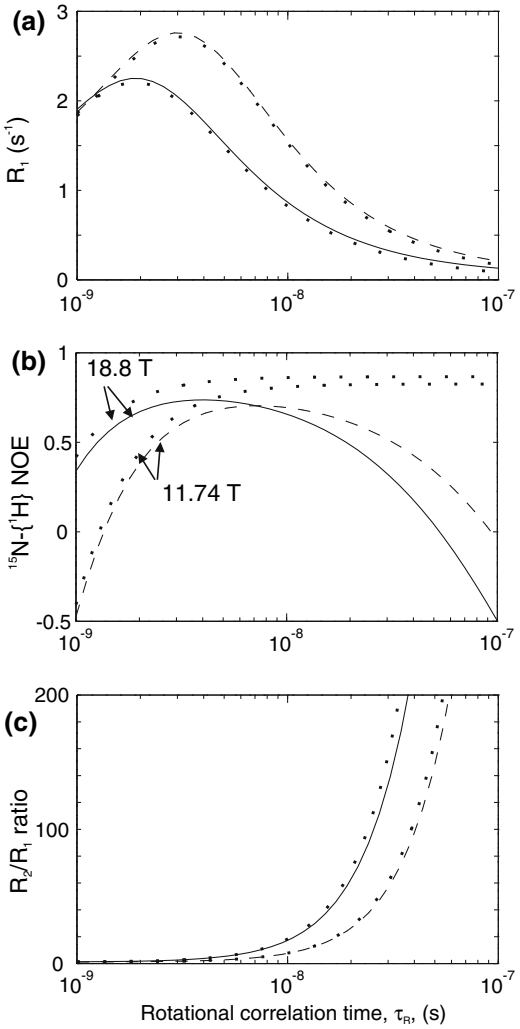

Fig. 2 (**a**) R_1, (**b**) ^{15}N–{^{1}H} NOE, and (**c**) R_2/R_1 ratio simulated at 18.8 T (solid line) and 11.74 T (dashed line) as a function of the rotational correlation time, τ_R. In each graph, the values are calculated assuming $J_{MF}(\omega)$ (solid or dashed lines) and $J_{SMF}(\omega)$ (dotted lines). Other simulation parameters are $S^2 = 0.85$, $\tau_i = 50$ ps, and $R_{ex} = 0$

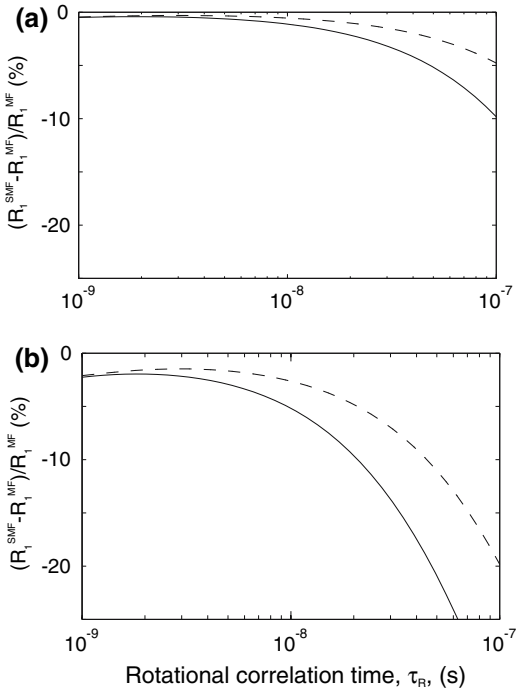

Fig. 3 Percentage difference of R_1 values, $(R_1^{SMF}–R_1^{MF})/R_1^{MF}$, assuming at (**a**) $\tau_i = 10$ ps and (**b**) 50 ps. Solid lines are those calculated at 18.8 T, and dashed lines are those calculated at 11.74 T. R_1^{SMF} and R_1^{MF} indicates R_1 values calculated using $J_{SMF}(\omega)$ and $J_{MF}(\omega)$, respectively. S^2 and R_{ex} were assumed to be 0.85 and 0, respectively

data typically contains larger uncertainties than those in R_1 and R_2 due to the lower sensitivity of the experiment, the more than 10% difference in the NOE values will clearly influence optimization of the model-free parameters. Such results indicate that many residues may not be fit using the $J_{SMF}(\omega)$ model when relaxation data is collected at the high magnetic field strength.

Parameter dependence of NOE values is shown in Eq. 9 (Kay et al. 1989).

$$\mathrm{NOE_{MF}} \approx \mathrm{NOE_{iso}} - \frac{50(1-S^2)}{(3+\delta)S^2}\tau_i\tau_m\omega_N^2 \qquad (9)$$

Here, $\mathrm{NOE_{MF}}$ is the NOE value calculated using $J_{MF}(\omega)$ given by Eq. 5, whereas $\mathrm{NOE_{iso}}$ indicates the NOE value under conditions of isotropic tumbling, i.e., at $S^2 = 1$. δ indicates ratio of chemical shift anisotropy and dipolar interaction, $(c/d)^2$. Equation 9 has been derived under the assumptions that $\omega_H \pm \omega_N \sim \omega_H$, $(\omega_H\tau_i)^2 \ll 1$ and $(\omega_N\tau_R)^2 \gg 1$ (Kay et al. 1989). Based on this equation, it is clear that NOE values will be reduced at higher magnetic field strengths or at slower rotational correlation times. Thus, when residues used for the estimation of the rotational correlation time are selected based on NOE values, such NOE cut-off should be set lower than usual for experiments conducted for large molecules at high field. This has the adverse effect that it becomes more difficult to distinguish variation in NOE values in rigid regions of proteins from reduced NOE values caused by slow internal motion.

R_2/R_1 values simulated using $J_{SMF}(\omega)$ and $J_{MF}(\omega)$

Based on the previous results that R_1^{SMF} is ca. 5% different from R_1^{MF} at 18.8 T and $\tau_R = 20$ ns, it is expected that R_2/R_1 values calculated using $J_{SMF}(\omega)$, R_2^{SMF}/R_1^{SMF}, would differ from those calculated using $J_{MF}(\omega)$, R_2^{MF}/R_1^{MF}. As shown in Fig. 2c, the R_2/R_1 ratio increases as a function of τ_R, which of course is due to the fact that R_2 increases and R_1 decreases as a function of τ_R. Figure 2c further shows

Table 1 Calculated relaxation values at various correlation times for internal motion[a]

τ_i (ps)	R_1 (s^{-1})	Diff. (%)[b]	R_2 (s^{-1})	Diff. (%)	NOE	Diff. (%)	R_2/R_1	Diff. (%)
11.74 T (500 MHz)								
0	0.816	–	22.50	–	0.821	–	27.5	–
10	0.824	–0.97	22.51	–0.04	0.777	5.66	27.3	0.732
20	0.833	–2.0	22.52	–0.09	0.733	12.0	27.0	1.85
30	0.841	–3.0	22.52	–0.09	0.691	18.8	26.8	2.61
18.8 T (800 MHz)								
0	0.423	–	29.19	–	0.865	–	69.0	–
10	0.431	–1.86	29.19	0	0.779	9.94	67.5	2.22
20	0.441	–4.06	29.20	–0.039	0.698	19.3	66.2	4.23
30	0.450	–6.3	29.23	–0.14	0.622	28.2	64.9	6.31

[a] Relaxation values were calculated assuming $S^2 = 0.85$ and $\tau_R = 20$ ns

[b] "Diff" indicates a fractional difference, $(X^{SMF} - X^{MF})/X^{MF}$. Here, X can be R_1, R_2, NOE, or R_2/R_1

Values at $\tau_i = 0$ corresponds to the case of $X^{SMF} = X^{MF}$

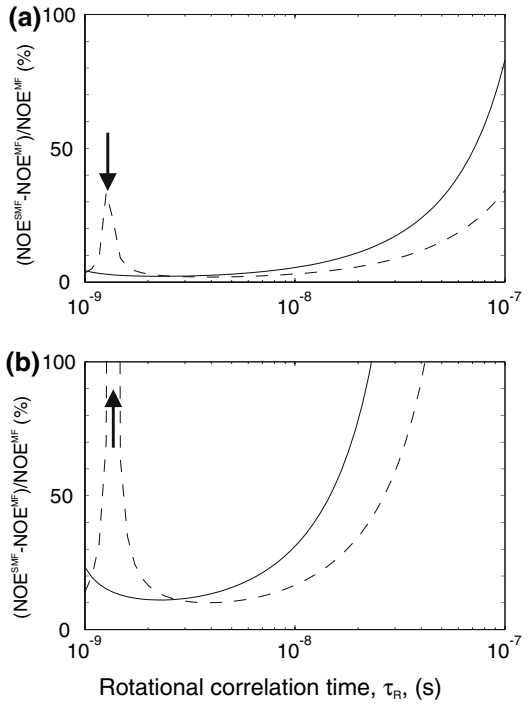

Fig. 4 Percentage difference of NOE values, $|\{(NOE^{SMF}–NOE^{MF})/NOE^{MF}\}|$, assuming at (**a**) $\tau_i = 10$ ps and (**b**) 50 ps. Arrows indicates the point that the sign of the NOE is changed. Solid lines are those calculated at 18.8 T, and dashed lines are those calculated at 11.74 T. NOE^{SMF} and NOE^{MF} indicates NOE values calculated using $J_{SMF}(\omega)$ and $J_{MF}(\omega)$, respectively. S^2 and R_{ex} were assumed to be 0.85 and 0, respectively

that the R_2^{SMF}/R_1^{SMF} values are slightly larger than R_2^{MF}/R_1^{MF} values, which is reasonable since R_1^{SMF} values are slightly smaller than R_1^{MF} (Fig. 2a) and since the R_2^{SMF} values are similar to the R_2^{MF} (Eqs. 2 and 8).

The differences in R_2/R_1 values, $\{(R_2^{SMF}/R_1^{SMF}) - (R_2^{MF}/R_1^{MF})\}/(R_2^{MF}/R_1^{MF})$, are less than 2% at $\tau_i = 10$ ps and $\tau_R = 10$ ns, at either 11.74 or 18.8 T (Fig. 5a). However, the discrepancy becomes more significant when $\tau_i = 50$ ps (Fig. 5b). When $\tau_R = 20$ ns at 18.8 T, the R_2/R_1 value calculated using $J_{SMF}(\omega)$ differs 9.4% from that calculated using $J_{MF}(\omega)$. Thus, when τ_R value is determined directly by calculating R_2^{SMF}/R_1^{SMF}, τ_R will be 4.6% underestimated. If S^2 is determined primarily by the contribution from the R_2 as suggested by Eqs. 2 and 8, then, it will be

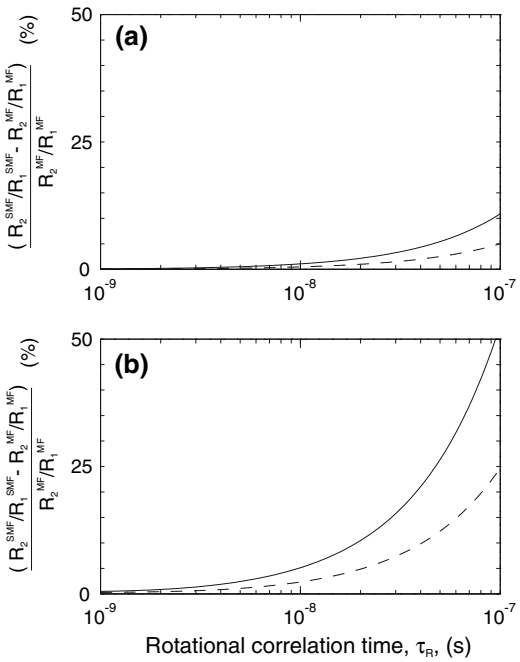

Fig. 5 Percentage difference of R_2/R_1 values, $(R_2^{SMF}/R_1^{SMF}–R_2^{MF}/R_1^{MF})/(R_2^{MF}/R_1^{MF})$, assuming at (**a**) $\tau_i = 10$ ps and (**b**) 50 ps. Solid lines are those calculated at 18.8 T, and dashed lines are those calculated at 11.74 T. S^2 and R_{ex} were assumed to be 0.85 and 0, respectively

overestimated due to the underestimation of τ_R. Thus, in the case of high field model-free analysis of larger proteins, it is suggested that τ_R values be estimated by fitting with $J_{MF}(\omega)$ for the sites closest to the trimmed mean R_2/R_1 value (Clore et al. 1990; Schneider et al. 1992) rather than by assuming $J_{SMF}(\omega)$.

Use of $J_{SMF}(\omega)$ at high magnetic field experiments for large proteins

Here, we show that R_1 and NOE values calculated using $J_{SMF}(\omega)$ become significantly different from those calculated using $J_{MF}(\omega)$ when the magnetic field strength or the rotational correlation time increases. When $J_{SMF}(\omega)$ is applied to optimize the model-free parameters at each amide site, the $S^2\tau_R/(1 + \omega_N^2\tau_R^2)$ term has to compensate for the neglect of the contribution from the $(1–S^2)\tau_e/(1 + \omega_H^2\tau_e^2)$ term in the $J_{MF}(\omega)$ spectral density, which results in an overestimation of S^2. Additionally, significant differences in R_1 will also influence the estimation of τ_R when it is directly calculated from the average R_2/R_1 ratio.

In practice, it is difficult to assess the accuracy of the optimized parameters when simplified model-free analysis is used to analyze very complicated protein dynamics (Andrec et al. 1999; Barchi et al. 1994; Chandrasekhar et al. 1992; Chen et al. 2004; d'Auvergne and Gooley 2003; Korchuganov et al. 2004; Korzhnev et al. 1997; Lee and Wand 1999; Meirovitch et al. 2003; Pawley et al. 2001; Schramm et al. 1991; Spyracopoulos 2006). In particular, contributions from R_{ex}, slow internal motion, and molecular anisotropy will each make evaluation of the R_2/R_1 ratio difficult. In addition, there are many factors that can influence the experimental values of heteronuclear NOE (Gong and Ishima 2007; Grzesiek and Bax 1993; Li and Montelione 1994; Renner et al. 2002; Skelton et al. 1993). Particularly, insufficient magnetization recovery will increase the NOE values, which in turn may cancel the reduction of NOE value caused by internal motion. Finally, even when $J_{MF}(\omega)$ model is applied for rigid sites, it is uncertain the extent to which $J_{MF}(\omega)$ differs from the actual spectral density at that site.

In spite of these difficulties, some of the published data, ubiquitin and TEM-1 in Table 2, clearly show a tendency that τ_R values estimated based on R_2/R_1 decrease as the magnetic field strength increases, which is consistent with our prediction. This reduction of the rotational correlation time estimated based on the $J_{SMF}(\omega)$ spectral density may reflect the difference between a real spectral density of a protein and $J_{MF}(\omega)$ spectral density. Although such differences are relatively small, 2–3%, for the data considered here, they might have a significant impact if the differences are directly reflected in the S^2 values. In contrast, the rotational correlation times of km23 (27 kDa homodimeric protein) estimated based on the $J_{MF}(\omega)$ spectral density increased as the magnetic field strength increased (Table 2), which may be due to residual chemical exchange contribution to R_2.

To avoid bias caused by R_1/R_2 ratio (or $J_{SMF}(\omega)$), the following strategies that are essentially free from the internal motion of each site may be applied when $\omega\tau_e << 1$.

$$J_{MF}(\omega) \cong S^2\frac{\tau_R}{(1+\omega^2\tau_R^2)} + (1-S^2)\tau_e = J_{SMF}(\omega) + (1-S^2)\tau_e \quad (10)$$

Using the notation shown in Eq. 10, relaxation rates are described by the following equations.

$$R_1^{MF} = R_1^{SMF} + (d^2+c^2)(1-S^2)\tau_e \quad (11)$$

$$R_2^{MF} = R_2^{SMF} + (d^2+7c^2/6)(1-S^2)\tau_e \quad (12)$$

$$\sigma_{cross}^{MF} = \sigma_{cross}^{SMF} + (d^2/2)(1-S^2)\tau_e \quad (13)$$

Based on these equations, an R_1/R_2 ratio that does not contain $(1–S^2)\tau_e$ term is derived.

$$\frac{R_2 - 2\sigma(d^2+7c_2/6)/d^2}{R_1 - 2\sigma(d^2+c_2)/d^2} = \frac{R_2^{SMF} - 2\sigma^{SMF}(d^2+7c_2/6)/d^2}{R_1^{SMF} - 2\sigma^{SMF}(d^2+c_2)/d^2} \quad (14)$$

This concept is recast in a simpler form using reduced spectral density function (Ishima and Nagayama 1995; Lefevre et al. 1996; Peng and Wagner 1995). Equation 10 clearly indicates that subtraction of the spectral density functions cancels out the $(1–S^2)\tau_e$ terms. Thus, τ_R is described by,

$$\tau_R = \left(\frac{(J(0)-J(\omega_N))}{(J(\omega_N)-J(\omega_H))}\cdot\frac{(0.87^*\omega_H-\omega_N)^2}{\omega_N^2} - 1\right)^{1/2}/\omega_H \quad (15)$$

The coefficient, 0.87, is a correction value in the reduced spectral density function (Pfeiffer et al. 2001). This equation is very similar to the equation previously derived (Fushman et al. 1994), but more generalized such that motion at ω_H does not affect τ_R (Fushman and Cowburn 2001). This equation is also similar to that described by Kroenke et al. (1998), but differs in that the $(1–S^2)\tau_e$ term is selectively removed rather than eliminating the entire $J(\omega_H)$ term. τ_R values were calculated using Eqs. 14 and 15 for km23 and TEM-1 (Table 2) and

Table 2 Rotational correlation times estimated using different methods[d,e]

km23 (Ilangovan et al. 2005)[a]	14.09 T	16.45 T	
Number of residues among total	39/83	37/83	
Average R_1	1.23 (0.066)	1.03 (0.045)	
Average R_2	13.64 (1.1)	15.75 (1.1)	
Average NOE	0.808 (0.038)	0.803 (0.049)	
τ_R estimated from R_2/R_1 ratio (ns)	10.25 (–)	10.45 (–)	
τ_R estimated from fit using J_{SMF} (ω) (ns)	10.25 (0.02)	10.45 (0.02)	
τ_R estimated from fit using J_{MF} (ω) (ns)	10.52 (0.05)	10.76 (0.03)	
τ_R estimated using Eq. 14	10.28 (0.05)	10.53 (0.03)	
τ_R estimated using Eq. 15	10.20	10.51	
Ubiquitin (Chang and Tjandra 2005)[b]	14.09 T	18.8 T	
Number of residues among total	53/64	38/63	
Average R_1	1.91 (0.066)	1.47 (0.038)	
Average R_2	7.60 (0.416)	8.70 (0.523)	
τ_R estimated from R_2/R_1 ratio (ns)	5.45 (0.19)	5.31 (0.20)	
τ_R estimated from fit using J_{SMF} (ω) (ns)	5.45 (0.04)	5.30 (0.05)	
TEM-1 (Savard and Gagne 2006)[c]	11.74 T	14.09 T	18.8 T
τ_R estimated from R_2/R_1 ratio (ns)	12.74	12.64	12.33
τ_R estimated from fit using J_{SMF} (ω) (ns)	12.7	12.5	–
τ_R estimated from fit using J_{MF} (ω) (ns)	12.82	12.76	–
τ_R estimated using Eq. 14	12.85	12.75	–
τ_R estimated using Eq. 15	12.93	12.80	–

[a] Km23 data published previously were used for the analysis (Ilangovan et al. 2005)

[b] Ubiquitin data are basically the same as published previously but obtained using ^{15}N protein (Chang and Tjandra 2005)

[c] TEM-1 data was obtained from the literature (Savard and Gagne 2006) and analyzed only using average R_1, R_2, and NOE values

[d] Numbers in parentheses in R_1, R_2, NOE, and τ_R values indicate uncertainty

[e] Residues for analysis were selected to satisfy the following four conditions (i) the NOE $>$ 0.7, (ii) R_1 is within 1.5 standard deviation, (iii) R_2/R_1 is within 1 standard deviation, and (iv) $(R_2-\langle R_2\rangle)/\langle R_2\rangle - (R_1-\langle R_1\rangle)/\langle R_1\rangle$ is smaller than 1.5 standard deviation. Since NOE values were not obtained for the ubiquitin data, residues for analysis for ubiquitin were selected to satisfy the above criteria, without (i) but using 0.5 standard deviation for (iii)

with the former were found to be close to those calculated using $J_{MF}(\omega)$, which is expected since these methods assume the same spectral density function. τ_R values calculated using the latter differed slightly from those calculated using $J_{MF}(\omega)$ presumably due inaccuracies in some of the assumptions used to derive the reduced spectral density function.

Acknowledgements We thank Dennis Torchia and Nico Tjandra for critical reading of the manuscript. Financial support for this work was provided by University of Pittsburgh to R.I., and the NIH and the Robert A. Welch Foundation to A.H.

References

Abu-Abed M, Millet O, MacLennan DH, Ikura M (2004) Probing nucleotide-binding effects on backbone dynamics and folding of the nucleotide-binding domain of the sarcoplasmic/endoplasmic-reticulum Ca^{2+}-ATPase. Biochem J 379:235–242

Andrec M, Montelione GT, Levy RM (1999) Estimation of dynamic parameters from NMR relaxation data using the Lipari-Szabo model-free approach and Bayesian statistical methods. J Magn Reson 139:408–421

Barchi JJJ, Grasberger B, Gronenborn AM, Clore GM (1994) Investigation of the backbone dynamics of the IgG-binding domain of streptococcal protein G by heteronuclear two-dimensional 1H-15N nuclear magnetic resonance spectroscopy. Protein Sci 3:15–21

Bouamr F, Cornilescu CC, Goff SP, Tjandra N, Carter CA (2005) Structural and dynamics studies of the D54A mutant of human T cell leukemia virus-1 capsid protein. J Biol Chem 280:6792–6801

Bruschweiler R (2003) New approaches to the dynamic interpretation and prediction of NMR relaxation data from proteins. Curr Opin Struct Biol 13:175–183

Campbell AP, Spyracopoulos L, Irvin RT, Sykes BD (2000) Backbone dynamics of a bacterially expressed peptide from the receptor binding domain of *Pseudomonas aeruginosa* pilin strain PAK from heteronuclear 1H-15N NMR spectroscopy. J Biomol NMR 17:239–255

Cavanagh J, Fairbrother WJ, Palmer AG, Skelton NJ (1996) Protein NMR spect. Academic Press, San Diego

Chandrasekhar I, Clore GM, Szabo A, Gronenborn AM, Brooks BR (1992) A 500 ps molecular dynamics simulation study of interleukin-1 beta in water. Correlation with nuclear magnetic

resonance spectroscopy and crystallography. J Mol Biol 226:239–250
Chang SL, Tjandra N (2005) Temperature dependence of protein backbone motion from carbonyl 13C and amide 15N NMR relaxation. J Magn Reson 174:43–53
Chen J, Brooks CLI, Wright PE (2004) Model-free analysis of protein dynamics: assessment of accuracy and model selection protocols based on molecular dynamics simulation. J Biomol NMR 29:243–257
Clore GM, D riscoll PC, Wingfield PT, Gronenborn AM (1990) Analysis of the backbone dynamics of interleukin-1 beta using two-dimensional inverse detected heteronuclear 15N-1H NMR spectroscopy. Biochemistry 29:7387–7401
Coles M, Diercks T, Muehlenweg B, Bartsch S, Zoelzer V, Tschesche H, Kessler H (1999) The solution strucuture and dynamics of human neutrophil gelatinase-associated lipocalin. J Mol Biol 289:139–157
d'Auvergne EJ, Gooley PR (2003) The use of model selection in the model-free analysis of protein dynamics. J Biomol NMR 25:25–39
Dayie KT, W agner G, Lefevre JF (1996) Theory and practice of nuclear spin relaxation in proteins. Annu Rev Phys Chem 47:243–282
Ding Z, Lee GI, Liang X, Gallazzi F, Arunima A, Van Doren SR (2005) PhosphoThr peptide binding globally rigidifies much of the FHA domain from Arabidopsis receptor kinase-associated protein phosphatase. Biochemistry 44:10119–10134
Farrow NA, Muhandiram R, Singer AU, Pascal SM, Kay CM, Gish G, Shoelson SE, Pawson T, Forman-Kay JD, Kay LE (1994) Backbone dynamics of a free and phosphopeptide-complexed Src homology 2 domain studied by 15N NMR relaxation. Biochemistry 33:5984–6003
Fausti S, Weiler S, Cuniberti C, Hwang KJ, No KT, Gruschus JM, Perico A, Nirenberg M, Ferretti JA (2001) Backbone dynamics for the wild type and a double H52R/T56W mutant of the vnd/NK-2 homeodomain from *Drosophila melanogaster*. Biochemistry 40:12004–12023
Fushman D, Cowburn D (2001) Nuclear magnetic resonance relaxation in determination of residue-specific N-15 chemical shift tensors in proteins in solution: protein dynamics, structure, and applications of transverse relaxation optimized spectroscopy. Nuclear Magnet Reson Biol Macromol Pt B:109–126
Fushman D, Tjandra N, Cowburn D (1999) An approach to direct determination of protein dynamics from N-15 NMR relaxation at multiple fields, independent of variable N-15 chemical shift anisotropy and chemical exchange contributions. J Am Chem Soc 121:8577–8582
Fushman D, Weisemann R, Thuring H, Ruterjans H (1994) Backbone dynamics of ribonuclease-T1 and its complex with BA 2'GMP studied by 2-dimensional heteronuclear NMR-spectroscopy S. J Biomol NMR 4:61–78
Garcia FL, Szyperski T, Dyer JH, Choinowski T, Seedorf U, Hauser H, Wuthrich K (2000) NMR structure of the sterol carrier protein-2: implications for the biological role. J Mol Biol 295:595–603
Gong Q, Ishima R (2007) 15N-{1H} NOE experiment at high magnetic field strengths. J Biomol NMR 37:147–157
Grzesiek S, Bax A (1993) The importance of not saturating H_2O in protein NMR – application to sensitivity enhancement and NOE measurements. J Am Chem Soc 115:12593
Idiyatullin D, Daragan VA, Mayo KH (2003) (NH)-N-15 backbone dynamics of protein GB1: comparison of order parameters and correlation times derived using various "model-free" approaches. J Phys Chem B 107:2602–2609
Igumenova TI, Frederick KK, Wand AJ (2006) Characterization of the fast dynamics of protein amino acid side chains using NMR relaxation in solution. Chem Rev 106:1672–1699
Ilangovan U, Ding W, Zhong Y, Wilson CL, Groppe JC, Trbovich JT, Zuniga J, Demeler B, Tang Q, Gao G, Mulder KM, Hinck AP (2005) Structure and dynamics of the homodimeric dynein light chain km23. J Mol Biol 352:338–354
Ishima R, Nagayama K (1995) Protein backbone dynamics revealed by quasi spectral density function analysis of amide N-15 nuclei. Biochemistry 34:3162–3171
Ishima R, Torchia DA (2000) Protein dynamics from NMR. Nat Struct Biol 7:740–743
Jarymowycz VA, Stone MJ (2006) Fast time scale dynamics of protein backbones: NMR relaxation methods, applications, and functional consequences. Chem Rev 106:1624–1671
Kay LE (2005) NMR studies of protein structure and dynamics. J Magn Reson 173:193–207
Kay LE, Torchia DA, Bax A (1989) Backbone dynamics of proteins as studied by nitrogen-15 inverse detected heteronuclear NMR spectroscopy: application to staphylococcal nuclease. Biochemistry 28:8972–8979
Korchuganov DS, Gagnidze IE, Tkach EN, Schulga AA, Kirpichnikov MP, Arseniev AS (2004) Determination of protein rotational correlation time from NMR relaxation data at various solvent viscosities. J Biomol NMR 30:431–442
Korzhnev DM, Orekhov VY, Arseniev AS (1997) Model-free approach beyond the borders of its applicability. J Biomol NMR 127:184–191
Kroenke CD, Loria JP, Lee LK, Rance M, Palmer AG (1998) Longitudinal and transverse H-1-N-15 dipolar N-15 chemical shift anisotropy relaxation interference: unambiguous determination of rotational diffusion tensors and chemical exchange effects in biological macromolecules. J Am Chem Soc 120:7905–7915
Lee AL, Wand AJ (1999) Assessing potential bias in the determination of rotational correlations times of proteins by NMR. J Biomol NMR 13:101–112
Lee LK, Rance M, Chazin WJ, Palmer AGr (1997) Rotational diffusion anisotropy of proteins from simultaneous analysis of 15N and 13C alpha nuclear spin relaxation. J Biomol NMR 9:287–298
Lefevre JF, Dayie KT, Peng JW, Wagner G (1996). Internal mobility in the partially folded DNA binding and dimerization domains of GAL4: NMR analysis of the N-H spectral density functions. Biochemistry 35:2674–2686
Li YC, Montelione GT (1994) Overcoming solvent saturation-transfer artifacts in protein Nmr at neutral Ph – application of pulsed-field gradients in measurements of H-1 N-15 overhauser effects. J Magnet Reson Ser B 105:45–51
Lipari G, Szabo A (1982) Model-free approach to the interpretation of nuclear magnetic resonance relaxation in macromolecules. 1. Theory and range of validity. J Am Chem Soc 104:4546–4559
Mandel AM, Akke M, Palmer AG (1995) Backbone dynamics of *Escherichia coli* ribonuclease Hi – correlations with structure and function in an active enzyme. J Mol Biol 246:144–163
Meirovitch E, Shapiro YE, Liang ZC, Freed JH (2003) Mode-coupling SRLS versus mode-decoupled model-free N-H bond dynamics: mode-mixing and renormalization. J Phys Chem B 107:9898–9904
Palmer AG 3rd (2001) Nmr probes of molecular dynamics: overview and comparison with other. Annu Rev Biophys Biomol Struct 30:129–155
Palmer AG, Rance M, Wright PE (1991) Intramolecular motions of a zinc finger DNA-binding domain from Xfin characterized by proton-detected natural abundance 13C heteronuclear NMR spectroscopy. J Am Chem Soc 113:4371–4380
Pawley NH, Wang C, Koide S, Nicholson LK (2001) An improved method for distinguishing between anisotropic tumbling and

chemical exchange in analysis of 15N relaxation parameters. J Biomol NMR 20:149–165

Pelupessy P, Ravindranathan S, Bodenhausen G (2003) Correlated motions of successive amide N–H bonds in proteins. J Biomol NMR 25:265–280

Peng JW, Wagner G (1995) Frequency spectrum of NH bonds in eglin c from spectral density mapping at multiple fields. Biochemistry 34:16733–16752

Pfeiffer S, Fushman D, Cowburn D (2001) Simulated and NMR-derived backbone dynamics of a protein with significant flexibility: a comparison of spectral densities for βARK1 PH domain. J Am Chem Soc 123:3021–3026

Philippopoulos M, Mandel AM, Palmer AGr, Lim C (1997) Accuracy and precision of NMR relaxation experiments and MD simulations for characterizing protein dynamics. Proteins 28:481–493

Redfield C (2004) Using nuclear magnetic resonance spectroscopy to study molten globule states of proteins. Methods Mol Biol 34:121–132

Renner C, Schleicher M, Moroder L, Holak TA (2002) Practical aspects of the 2D N-15-{H-1}-NOE experiment. J Biomol NMR 23:23–33

Savard PY, Gagne SM (2006) Backbone dynamics of TEM-1 determined by NMR: evidence for a highly ordered protein. Biochemistry 45:11414–11424

Schneider DM, Dellwo MJ, Wand AJ (1992) Fast internal main-chain dynamics of human ubiquitin. Biochemistry 31:3645–3652

Schramm HJ, Nakashima H, Schramm W, Wakayama H, Yamamoto N (1991) HIV-1 reproduction is inhibited by peptides derived from the N- and C-termini. Biochem Biophys Res Commun 179:847–851

Sheinerman FB, Brooks CLr (1997) A molecular dynamics simulation study of segment B1 of protein G. Proteins 29:193–202

Skelton NJ, Palmer AG, Akke M, Kordel J, Rance M, Chazin WJ (1993) Practical aspects of 2-dimensional proton-detected N-15 spin relaxation measurements. J Magnet Reson Ser B 102:253–264

Spyracopoulos L (2006) A suite of mathematica notebooks for the analysis of protein main chain (15)N NMR relaxation data. J Biomol NMR 36:215–224

Stone M, Chandrasekhar K, Holmgren A, Wright PE, Dyson HJ (1993) Abstract comparison of backbone and tryptophan side-chain dynamics of reduced and oxidized *Escherichia coli* thioredoxin using 15N NMR relaxation measurements. Biochemistry 32:426–435

Tjandra N, Kuboniwa H, Ren H, Bax A (1995) Rotational dynamics of calcium-free calmodulin studied by 15N-NMR relaxation measurements. Eur J Biochem 230:1014–1024

Yuan P, Marshall VP, Petzold GL, Poorman RA, Stockman BJ (1999) Dynamics of stromelysin/inhibitor interactions studied by 15N NMR relaxation measurements: comparison of ligand binding to the S1-S3 and S1-S3 subsites. J Biomol NMR 15:55–64

Zhuravleva AV, Korzhnev DM, Kupce E, Arseniev AS, Billeter M, Orekhov VYY (2004) Gated electron transfers and electron pathways in azurin: a NMR dynamic study at multiple fields and temperatures. J Mol Biol 342:1599–1611